An Interatomic Potential of Li-Mn-O System and Molecular Dynamics Simulations on Li Diffusion in Spinel $Li_{1-x}Mn_2O_4$

Eunkoo Lee,[1] Kwang-Ryeol Lee,[2] Byeong-Joo Lee[1,*]

[1]Department of Materials Science and Engineering,
Pohang University of cience and Technology (POSTECH), Pohang 37673, Republic of Korea
[2]Computational Science Center,
Korea Institute of Science and Technology, Seoul 02792, Republic of Korea

SUPPLEMENT

1. Formalism of the Second Nearest-Neighbor Modified Embedded-Atom Method Interatomic Potentials

A. 2NN MEAM formalism for pure elements

In the MEAM, the total energy of a system is approximated as

$$E = \sum_i \left[F_i(\overline{\rho}_i) + \frac{1}{2} \sum_{j(\neq i)} S_{ij} \phi_{ij}(R_{ij}) \right] \qquad \text{(1-A1)}$$

where F_i is the embedding function, $\overline{\rho}_i$ is the background electron density at site i. S_{ij} and ϕ_{ij} (R_{ij}) are the screening factor and the pair interaction between atoms i and j separated by a distance R_{ij}, respectively. For general calculations of energy, the functional forms for the two terms on the right hand side of Eq.(1), F_i and ϕ_{ij}, should be given. The background electron density at a site is computed considering directionality in bonding. A specific form is given to the embedding function F_i, but not to the pair interaction ϕ_{ij}. Instead a reference structure where individual atoms are on the exact lattice points is defined and the total energy per atom of the reference structure is estimated from the zero-temperature universal equation of state of Rose et al.[1] Then, the value of the pair interaction is evaluated from the known values of the total energy per atom and the embedding energy, as a function of nearest-neighbor distance. In the original MEAM[2], only first nearest-neighbor interactions are considered. The neglect of the second nearest-neighbor and more distant nearest-neighbor interactions is made effective by the use of a strong many-body screening function[3]. The consideration of the second nearest-neighbor

interactions in the modified formalism (the second nearest-neighbor MEAM[4–7]) is effected by adjusting the screening parameters so that the many-body screening becomes less severe.

It has been shown in Eq.(1-A1) that the energy in the MEAM is composed of two terms, the embedding function term and the pair interaction term. The embedding function is given the following form (1-A2),

$$F(\bar{\rho}) = AE_c \frac{\bar{\rho}}{\bar{\rho}^o} \ln \frac{\bar{\rho}}{\bar{\rho}^o} \qquad \text{(1-A2)}$$

where A is an adjustable parameter, E_c is the cohesive energy and $\bar{\rho}^o$ is the background electron density for a reference structure. The reference structure is a structure where individual atoms are on the exact lattice points. Normally, the equilibrium structure is taken as the reference structure for elements. The background electron density $\bar{\rho}_i$ is composed of spherically symmetric partial electron density, $\rho_i^{(0)}$, and angular contributions, $\rho_i^{(1)}$, $\rho_i^{(2)}$, $\rho_i^{(3)}$. Each partial electron density term has the following form,

$$(\rho_i^{(0)})^2 = \left[\sum_{j \neq i} S_{ij} \rho_j^{a(0)}(R_{ij}) \right]^2 \qquad \text{(1-A3a)}$$

$$(\rho_i^{(1)})^2 = \sum_{\alpha} \left[\sum_{j \neq i} \frac{R_{ij}^{\alpha}}{R_{ij}} S_{ij} \rho_j^{a(1)}(R_{ij}) \right]^2 \qquad \text{(1-A3b)}$$

$$(\rho_i^{(2)})^2 = \sum_{\alpha,\beta} \left[\sum_{j \neq i} \frac{R_{ij}^{\alpha} R_{ij}^{\beta}}{R_{ij}^2} S_{ij} \rho_j^{a(2)}(R_{ij}) \right]^2 - \frac{1}{3} \left[\sum_{j \neq i} S_{ij} \rho_j^{a(2)}(R_{ij}) \right]^2 \qquad \text{(1-A3c)}$$

$$(\rho_i^{(3)})^2 = \sum_{\alpha,\beta,\gamma} \left[\sum_{j \neq i} \frac{R_{ij}^{\alpha} R_{ij}^{\beta} R_{ij}^{\gamma}}{R_{ij}^3} S_{ij} \rho_j^{a(3)}(R_{ij}) \right]^2 - \frac{3}{5} \sum_{\alpha} \left[\sum_{j \neq i} \frac{R_{ij}^{\alpha}}{R_{ij}} S_{ij} \rho_j^{a(3)}(R_{ij}) \right]^2 \qquad \text{(1-A3d)}$$

Here, $\rho_j^{a(h)}$ represent atomic electron densities from j atom at a distance R_{ij} from site i. $R_{ij}{}^{\alpha}$ is the α component of the distance vector between atoms j and i ($\alpha = x, y, z$). The expression for $(\rho_i^{(3)})^2$ (Eq.(1-A3d)) is that modified later in order to make the partial electron densities orthogonal (1-A4). The way of combining the partial electron densities to give the total background electron density is not unique, and several expressions have been proposed[3]. Among them, the following form that can be widely used without numerical error is taken in the present work.

$$\bar{\rho}_i = \rho_i^{(0)} G(\Gamma) \qquad \text{(1-A4)}$$

where

$$G(\Gamma) = \frac{2}{1 + e^{-\Gamma}} \qquad \text{(1-A5)}$$

and

$$\Gamma = \sum_{h=1}^{3} t_i^{(h)} \left[\frac{\rho_i^{(h)}}{\rho_i^{(0)}} \right]^2 \qquad \text{(1-A6)}$$

$t_i^{(h)}$ are adjustable parameters. The atomic electron density is given as,

$$\rho_j^{a(h)}(R) = \rho_0 e^{-\beta^{(h)}(R/r_e - 1)} \qquad \text{(1-A7)}$$

where ρ_0 is a scaling factor, $\beta^{(h)}$ are adjustable parameters and r_e is the nearest-neighbor distance in the equilibrium reference structure. The scaling factor doesn't give any effect on calculations for elements, but can give effect on calculations for alloy systems.

In the MEAM no specific functional expression is given directly to $\phi(R)$. Instead, the atomic energy (total energy per atom) is evaluated by some means as a function of nearest-neighbor distance. Then, the value of $\phi(R)$ is computed from known values of the total energy and the embedding energy, as a function of nearest-neighbor distance.

Let's consider a reference structure once again. Here, every atom has the same environment and the same energy. If up to second nearest-neighbor interactions are considered as is done in the 2NN MEAM[4,5], the total energy per atom in a reference structure can be written as follows:

$$E^a(R) = F(\bar{\rho}^o(R)) + \frac{Z_1}{2}\phi(R) + \frac{Z_2 S}{2}\phi(aR) \qquad \text{(1-A8)}$$

where Z_1 and Z_2 are the number of first and second nearest-neighbor atoms, respectively. S is the screening factor for second nearest-neighbor interactions (the screening factor for first nearest-neighbor interactions is 1), and a is the ratio between the second and first nearest-neighbor distances. It should be noted that for a given reference structure S and a are constants, and the total energy and the embedding energy become functions of only nearest-neighbor distance R. On the other hand, the energy per atom for a reference structure can be obtained from the zero-temperature universal equation of state of Rose et al.[1] as a function of nearest-neighbor distance R.

$$E^u(R) = -E_c(1 + a^* + da^{*3})e^{-a^*} \qquad \text{(1-A9)}$$

where d is an adjustable parameter, and

$$a^* = \alpha(R/r_e - 1) \qquad \text{(1-A10)}$$

and

$$\alpha = \left(\frac{9B\Omega}{E_c} \right)^{1/2}. \qquad \text{(1-A11)}$$

$E^u(R)$ is the universal function for a uniform expansion or contraction in the reference structure, B is the bulk modulus and Ω is the equilibrium atomic volume.

Basically, the pair potential between two atoms separated by a distance R, $\phi(R)$, can be obtained by equating Eq.(1-A8) and Eq.(1-A9). However, it is not trivial because Eq.(1-A8) contains two pair potential terms. In order to derive an expression for the pair interaction, $\phi(R)$, another pair potential, $\psi(R)$, is introduced:

$$E^u(R) = F(\bar{\rho}^o(R)) + \frac{Z_1}{2}\psi(R) \qquad \text{(1-A12)}$$

where

$$\psi(R) = \phi(R) + \frac{Z_2 S}{Z_1}\phi(aR). \qquad \text{(1-A13)}$$

$\psi(R)$ can be computed from Eq.(1-A11) as a function of R, as follows:

$$\psi(R) = \frac{2}{Z_1}[E^u(R) - F(\bar{\rho}^o(R))], \qquad \text{(1-A14)}$$

and the expression for the pair potential $\phi(R)$ is obtained from Eq.(1-A12) as follows:

$$\phi(R) = \psi(R) + \sum_{n=1}(-1)^n\left(\frac{Z_2 S}{Z_1}\right)^n \psi(a^n R). \qquad \text{(1-A15)}$$

Here, the summation is performed until a correct value of atomic energy is obtained for the equilibrium reference structure.

It should be noted here that the original first nearest neighbor MEAM is a special case ($S = 0$) of the present 2NN MEAM. In the original MEAM, the neglect of the second nearest-neighbor interactions is made by the use of a strong many-body screening function[3]. In the same way, the consideration of the second nearest-neighbor interactions in the modified formalism is effected by adjusting the many-body screening function so that it becomes less severe. In the MEAM, the many-body screening function between atoms i and j, S_{ij}, is defined as the product of the screening factors, S_{ikj}, due to all other neighbor atoms k:

$$S_{ij} = \prod_{k \neq i,j} S_{ikj} \qquad \text{(1-A16)}$$

The screening factor S_{ikj} is computed using a simple geometric construction. Imagine an ellipse on an x, y plane, passing through atoms, i, k and j with the x-axis of the ellipse determined by atoms i and j.

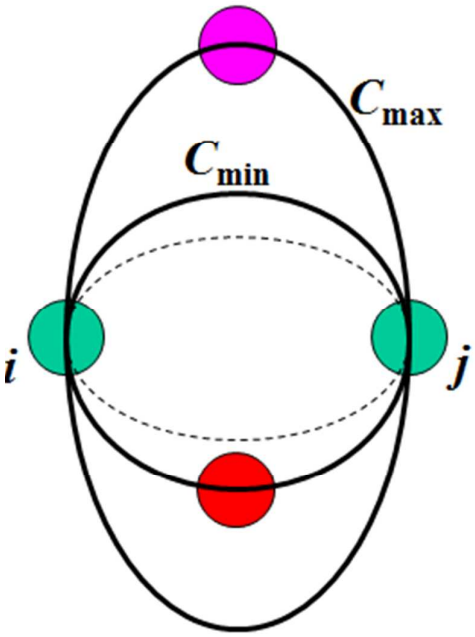

The equation of the ellipse is given by,

$$x^2 + \frac{1}{C}y^2 = \left(\frac{1}{2}R_{ij}\right)^2 . \qquad \text{(1-A17)}$$

For each k atom, the value of parameter C can be computed from relative distances among the three atoms, i, j and k, as follows:

$$C = \frac{2(X_{ik} + X_{kj}) - (X_{ik} - X_{kj})^2 - 1}{1 - (X_{ik} - X_{kj})^2} \qquad \text{(1-A18)}$$

where $X_{ik}=(R_{ik}/R_{ij})^2$ and $X_{kj}=(R_{kj}/R_{ij})^2$. The screening factor, S_{ikj} is defined as a function of C as follows:

$$S_{ikj} = f_c\left[\frac{C - C_{\min}}{C_{\max} - C_{\min}}\right] \qquad \text{(1-A19)}$$

where C_{min} and C_{max} are the limiting values of C determining the extent of screening and the smooth cutoff function is

$$f_c(x) = \begin{cases} 1 & x \geq 1 \\ \left[1 - (1-x)^4\right]^2 & 0 < x < 1 \\ 0 & x \leq 0. \end{cases} \qquad \text{(1-A20)}$$

The basic idea for the screening is as follows: First define two limiting values, C_{max} and C_{min} ($C_{max} > C_{min}$). Then, if the atom k is outside of the ellipse defined by C_{max}, it is thought that the atom k does not have any effect on the interaction between atoms i and j. If the atom k is inside of the ellipse defined by C_{min} it is thought that the atom k completely screens the i-j interaction, and between C_{max} and C_{min} the screening changes gradually. In the numerical procedure of simulation the electron density and pair potential are multiplied by the screening function S_{ij}, as in done in Eq.(1-A1) and Eqs.(1-A3a)-(1-A3d). Therefore, $S_{ij}=1$ and $S_{ij}=0$ mean that the interaction between atoms i and j is unscreened and completely screened, respectively. In addition to the many-body screening function, a radial cutoff function which is given by $f_c[(r_c - r)/\Delta r]$ where r_c is the cutoff distance and Δr (0.1 Å) is the cutoff region, is also applied to the atomic electron density and pair potential[3]. The radial cutoff distance is chosen so that it doesn't have any effect on the calculation results due to the many-body screening. This is only for the computational convenience, that is, to save the computation time.

B. 2NN MEAM formalism for binary systems

To describe a binary alloy system, in addition to the descriptions for individual elements, the pair interaction between different elements should be determined. For this, a similar technique used to determine the pair interaction for pure elements is applied. A perfectly ordered binary intermetallic compound, where one type of atom has only same type of atoms as second nearest-neighbors, is considered as a reference structure. The Bl (NaCl type) or B2 (CsCl type) ordered structure can be a good example. For such a reference structure, the total energy per atoms (for l/2 *i* atom + 1/2 *j* atom) is given as follows:

$$E_{ij}^{u}(R) = \frac{1}{2}\left[F_i(\overline{\rho}_i) + F_j\left(\overline{\rho}_j\right) + Z_1\phi_{ij}(R) + \frac{Z_2}{2}\left(S_i\phi_{ii}(aR) + S_j\phi_{jj}(aR)\right)\right] \qquad \text{(1-B1)}$$

where Z_1 and Z_2 are the numbers of first and second nearest-neighbors in the reference structure, respectively. S_i and S_j are the screening functions for the second nearest-neighbor interactions between *i* atoms and between *j* atoms, respectively, and *a* is the ratio between the second and first nearest-neighbor distances in the reference structure. The pair interaction between *i* and *j* can now be obtained in the following form:

$$\phi_{ij}(R) = \frac{1}{Z_1}\left[2E_{ij}^{u}(R) - F_i(\overline{\rho}_i) - F_j(\overline{\rho}_j) - \frac{Z_2}{2}\left(S_i\phi_{ii}(aR) + S_j\phi_{jj}(aR)\right)\right]. \qquad \text{(1-B2)}$$

The embedding functions F_i and F_j can be readily computed. The pair interactions ϕ_{ii} and ϕ_{jj} between the same types of atoms can also be computed from descriptions of individual elements. To obtain $E_{ij}^{u}(R)$, the universal equation of state, Eqs.(1-A9)-(1-A11), is considered once again for the binary reference structure. In this case, E_c, r_e and B correspond to the cohesive energy, equilibrium nearest-neighbor distance and bulk modulus of the binary reference structure.

In addition to the parameters for the universal equation of state, two more model parameter groups, C_{min} and C_{max}, must be determined to describe alloy systems. Each element has its own value of C_{min} and C_{max}. C_{min} and C_{max} determine the extent of screening of an atom (*k*) to the interaction between two neighboring atoms (*i* and *j*). For pure elements, the three atoms are all the same type (*i*-*j*-*k* = A-A-A or B-B-B). However, in the case of binary alloys, one of the interacting atoms and/or the screening atoms can be different types (there are four cases: *i*-*k*-*j* = A-B-A, B-A-B, A-A-B and A-B-B). Different C_{min} and C_{max} values may have to be given in each case. Another, the last model parameter necessary for binary alloy systems is the atomic electron density scaling factor ρ_o (see Eq.(1-A7)). For an equilibrium reference structure ($R = r_e$), the values of all atomic electron densities become ρ_o. This is an arbitrary value and does not have any effect on calculations for pure elements. This parameter is often omitted when describing the potential model for pure elements. However, for alloy systems, especially for systems where the constituent elements have different coordination numbers, the scaling factor (the ratio of the two values) has a great effect on calculations.

C. 2NN MEAM formalism for multicomponent systems

The MEAM potential for a multicomponent alloy system is based on the MEAM for sub-unary and lower order alloy systems. As has been shown above, a binary system is described based on fourteen potential parameters of each element and thirteen binary parameters. The MEAM potential for a ternary system is obtained by combining all sub-unary and binary parameters. In addition, three more ternary parameters for each of C_{min}(i-k-j) and C_{max}(i-k-j) are necessary. Generally, information on the fundamental physical properties of ternary systems is rare and it is not easy to uniquely determine the ternary C_{min}(i-k-j) and C_{max}(i-k-j) values. In order to skip the procedure where one has to determine ternary potential parameter values without enough amount of ternary information, some assumptions are made for the ternary C_{min}(i-k-j) and C_{max}(i-k-j) values based on binary parameters. For example, in the case of Fe-Ti-C (or N) ternary system, it is considered that two elements, Fe and Ti, are relatively similar to each other compared to interstitial atoms such as C or N. It is assumed that the degree of screening by a C atom to the interaction between Fe and Ti atoms [C_{min} and C_{max}(Fe-C-Ti)] is an average between those to the Fe-Fe [C_{min} and C_{max}(Fe-C-Fe)] and Ti-Ti [C_{min} and C_{max}(Ti-C-Ti)] interactions. Similarly, the degree of screening by an Fe (or Ti) atom to the interaction between Ti (or Fe) and C atoms [C_{min} and C_{max}(Ti-Fe-C) or C_{min} and C_{max}(Fe-Ti-C)] is assumed to be an average between those by an Fe atom to the Fe-C [C_{min} and C_{max}(Fe-Fe-C)] and by a Ti atom to the Ti-C [C_{min} and C_{max}(Ti-Ti-C)] interactions. These assumptions have been introduced to the MEAM potential of Fe-Ti-C, Fe-Ti-N[8], Fe-Nb-C and Fe-Nb-N[9] ternary systems, found to result in reasonable descriptions of interfacial properties between Fe matrix and TiC, NbC carbides or TiN, NbN nitrides and are now adapted as a first approximation to estimate the ternary C_{min}(i-k-j) and C_{max}(i-k-j) parameter values when decisive information on ternary properties is not available.

2. Formalism of 2NNMEAM+Qeq Interatomic Potential Model

A. Total energy

The formalism of the potential proposed in the present study contains two terms, non-electrostatic and electrostatic interaction terms. The non-electrostatic interaction term is exactly identical to the existing 2NNMEAM potential formalism and is independent from atomic charges. The electrostatic interaction term is a function of atomic positions and charges. Therefore, the total energy of the system including N atoms is expressed as

$$E^{Total} = E^{MEAM}(\mathbf{x}) + E^{ES}(\mathbf{x}, \mathbf{q}) \qquad \text{(2-A1)}$$

where $\mathbf{x}=\{\mathbf{x}_1, \mathbf{x}_2, \ldots, \mathbf{x}_N\}$ and $\mathbf{q}=\{q_1, q_2, \ldots, q_N\}$ is a variable set of atomic positions and charges, respectively. The non-electrostatic and electrostatic terms are independent of each other. The 2NNMEAM energy of the reference structure basically satisfies the Rose universal equation of state (EOS)[1,10] which describes well a universal relationship between the total energy and interatomic distances in metallic and covalent solids. It is known that the Rose equation does not describe well the ionic solids. However, even in the case of ionic solids, it has been pointed out that the Rose equation is applied well if the electrostatic interaction term is considered separately[11,12]. Therefore, in the present formalism, the 2NNMEAM terms based on the Rose EOS is used without any modification and only the electrostatic term is newly introduced. Details of the 2NNMEAM formalism will not be given here. Readers are referred to Refs.[4,7].

The electrostatic energy is expressed by the sum of atomic energy E_i^{atom} and Coulomb pair interaction V_{ij}^{Coul}, using terminology of Rappe and Goddard[13]:

$$E^{ES} = \sum_i^N E_i^{atom}(q_i) + \sum_{i,j(i\neq j)}^N \frac{1}{2} V_{ij}^{Coul}\left(q_i, q_j, R_{ij}\right) \qquad \text{(2-A2)}$$

where R_{ij} represents interatomic distance between atom i and j.

a. Atomic energy

Rappe and Goddard[13] expressed the atomic energy of an atom i as a quadratic polynomial of atomic charge q_i,

$$E_i^{atom}(q_i) = \chi_i^0 q_i + \tfrac{1}{2} J_i^0 q_i^2 \qquad \text{(2-A3)}$$

Here, χ_i^0 is the electronegativity and J_i^0 is the atomic hardness or the self-Coulomb repulsion. It has been pointed out that this simple quadratic polynomial atomic energy term does not yield a sufficient amount of penalty energy enough to prevent atoms from being unreasonably charged beyond the charge limits. Once the atomic penalty energy fails to keep the atomic charge within a given limit, the Coulomb interaction term becomes increasingly high as cationic and anionic atoms get closer to each other. The electrostatic attractive force between the two oppositely charged ions becomes stronger and the distance between the two ions becomes even shorter as the molecular dynamics time step proceeds, and the atomic structure of the ionic crystal eventually collapses. To prevent this charge instability problem, Rappe and Goddard assign limits to atomic charges and adjust the charge values whenever any equilibrium charges are calculated to go beyond the limits.

In the present study, the atomic energy term is defined in a way to overcome simultaneously the charge instability problem and also to keep the minimization problem linear. While the original Qeq method uses a quadratic function defined for the overall range of the charge state, in the present study, the possible charge state is divided into several ranges and a quadratic polynomial is defined for each range of the charge state. That is,

$$E_i^{atom(1)}(q_i) = \tfrac{1}{2} J_i^0 q_i^2 + \chi_i^0 q_i \qquad (0 < |q_i| < 1e) \quad \text{(2-A4a)}$$

$$E_i^{atom(2)}(q_i) = a_i^{(2)} q_i^2 + b_i^{(2)} q_i + c_i^{(2)} \qquad (1e < |q_i| < 2e) \quad \text{(2-A4b)}$$

$$E_i^{atom(3)}(q_i) = a_i^{(3)} q_i^2 + b_i^{(3)} q_i + c_i^{(3)} \qquad (2e < |q_i| < 3e) \quad \text{(2-A4c)}$$

$$E_i^{atom(4)}(q_i) = a_i^{(4)} q_i^2 + b_i^{(4)} q_i + c_i^{(4)} \qquad (3e < |q_i| < 4e) \quad \text{(2-A4d)}$$

The functional form of $E_i^{\text{atom}(1)}$ is exactly the same as the atomic energy term in the original Qeq method, but its domain of definition is [0, 1e]. For $|q_i|$ in the range of [1e, 2e], the atomic

energy is defined by another quadratic polynomial, $E_i^{\mathrm{atom}(2)}$. This second atomic energy term is set to be smoothly continuous at $|q_i|=1e$ with the first atomic energy term and to be larger than the first atomic energy term in the given range, [1e, 2e]. The third and fourth atomic energy terms can be defined in the same way. Namely, a quadratic spline function is used in the present study as the atomic energy term. In order to determine each quadratic uniquely, one more condition is required in addition to the continuity and smoothness. The condition is defined by introducing parameters,

$$\Delta E_i^{(n)} = E_i^{atom(n)}(\pm n) - E_i^{atom(n-1)}(\pm n) \quad (n = 2,3,4) \qquad \text{(2-A5)}$$

Positive signs are taken for cationic elements and negative signs for anionic elements. Using $\Delta E_i^{(n)}$, the coefficients in equations (A-4a)-(2-4d) can be determined recursively. That is,

$$a_i^{(n)} = a_i^{(n-1)} + \Delta E_i^{(n)} \qquad \text{(2-A6a)}$$

$$b_i^{(n)} = b_i^{(n-1)} \mp 2(n-1)\Delta E_i^{(n)} \qquad \text{(2-A6b)}$$

$$c_i^{(n)} = c_i^{(n-1)} + (n-1)^2 \Delta E_i^{(n)} \qquad \text{(2-A6c)}$$

where $a_i^{(1)} = \frac{1}{2}J_i^0$, $b_i^{(1)} = \chi_i^0$, $c_i^{(1)} = 0$ and n = 2, 3, 4. By choosing positive values for $\Delta E_i^{(n)}$, the atomic energy for higher charge state can be always lager than that for lower charge state.

The relation between atomic energy and atomic charge is illustrated in the following figure. $\Delta E_i^{(n)}$ (n = 2, 3, 4) are newly introduced potential parameters that prevent the charge instability and also have an effect on other properties. The present approach requires an additional process to check whether computed equilibrium charges of individual cationic atoms remain in the initially assigned charge range. Details of this issue will also be described in section c.

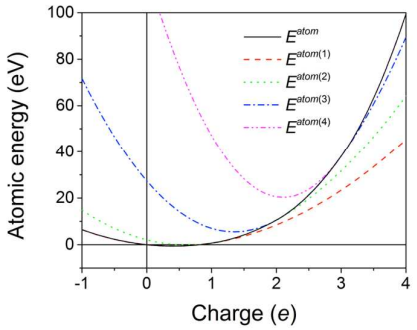

b. Coulomb interaction & long-range summation

In the original Qeq method[13], Coulomb interactions between two charged atoms are represented by a Coulomb integral between atomic densities of ns-Slater orbital. For large separations, the Coulomb interaction between unit charges on centers of two atoms separated by a distance R is k_c/R exactly as in the case of two point charges, where k_c is the Coulomb constant. As $R \rightarrow 0$, however, the charge distributions on the two atoms overlap and the Coulomb interaction should converge to a finite value by a shielding effect. There are a number of ways of evaluating the shielding of two charge distributions. This is related to the functional form of atomic densities or charge distributions. While Rappe and Goddard choose the ns-Slater orbital as the atomic density function, the Zhou potential[14] and COMB3[15] use an atomic density function of the form

$$\rho_i(r; q_i) = Z_i \delta(r) + (q_i - Z_i) f_i(r) \qquad \text{(2-A7)}$$

which is first proposed by Streitz and Mintmire[16]. Z_i is an effective core charge and f_i the radial distribution function of the valence charge. The function $f_i(r)$ can be expressed by a simple exponential function (the density function of 1s Slater orbital):

$$f_i(r) = \frac{\zeta_i^3}{\pi} \exp(-2\zeta_i r) \qquad \text{(2-A8)}$$

where the parameter ζ_i controls the spread of the electron distribution. The Coulomb integral between two atomic densities can be written

$$V_{ij}^{Coul}(q_i, q_j, R_{ij}) = k_c \iint \frac{\rho_i(r_i, q_i)\rho_j(r_j, q_j)}{|\mathbf{r}_i - \mathbf{r}_j|} d^3\mathbf{r}_i d^3\mathbf{r}_j \qquad \text{(2-A9)}$$

In the present study, the atomic density function of Streitz and Mintmire, Eq. (2-A7), is used because of its mathematical simplicity. The analytic solution of double integral in Eq. (2-A9) is as derived by Zhou et al.[14] and summarized also in section B-a.

As mentioned already, for large separations, the Coulomb interaction converges to k_c/R which is a long-range interaction. Classically, this long-range interaction can be evaluated using the well-known Ewald summation technique[17] which has been used in the original Qeq and Zhou potentials. The Ewald summation technique accurately computes long-range interactions. However, the computational cost is expensive due to the Fourier transform involved in the summation procedure. The COMB3 uses the charge-neutralized real-space direct summation method[18] (Wolf's direct summation method hereafter) which computes the long-range Coulomb potential without using the Fourier transform. The computational cost of Wolf's direct summation method is relatively low because the Fourier transform is not necessary. However, this method involves a probable computational error. According to Wolf et al.[18], the calculation for a perfect crystal can be evaluated almost accurately in comparison with Ewald summation. They report that even in the case of highly disordered systems, the amount of error is negligible. In molecular dynamic simulations, a highly efficient calculation with an acceptable amount of error is preferable to an exact calculation with an expensive computational cost. Therefore, the Wolf's direct summation is used in the present study instead of the Ewald summation.

The double integral for Coulomb integration in Eq. (2-A9) involves one long-range $1/R$ term, and the other exponential terms included are of short-range. The short-range exponential terms effectively decay at relatively short distances, and therefore, can be directly summed up. The lattice summation of $1/R$ term is replaced by

$$\frac{1}{2}\sum_{i,j(i\neq j)}^{N} k_c \frac{q_i q_j}{R_{ij}} \approx \frac{1}{2}\sum_{i,j(i\neq j)}^{N} k_c q_i q_j \left(\frac{\mathrm{erfc}(\alpha R_{ij})}{R_{ij}} - \frac{\mathrm{erfc}(\alpha R_c)}{R_c}\right) - \sum_{i}^{N} k_c q_i^2 \left(\frac{\mathrm{erfc}(\alpha R_c)}{2R_c} + \frac{\alpha}{\sqrt{\pi}}\right) \tag{2-A10}$$

in the Wolf's direct summation method as described in B.2. Here, α is the damping coefficient and R_c is the cutoff radius. As α increases, the Coulomb potential converges at shorter cutoff radius but the error increases, and vice versa. Therefore, it is necessary to determine an optimized value of α and R_c considering computational accuracy and efficiency. By several tests, α=0.2 Å^{-1} and R_c=12 Å are finally selected in this study.

c. Minimization method

The analytic form of the total electrostatic energy, Eq. (2-A2), is now clearly defined as a function of atomic positions and charges. For any form of quadratic function of q_i's, one can generalize the total electrostatic energy as

$$E_{total}^{ES} = \sum_i^N q_i\chi_i + \frac{1}{2}\sum_{i,j}^N q_i q_j J_{ij} \qquad \text{(2-A11)}$$

where χ_i and J_{ij} are coefficients independent of q_i. In this study, χ_i and J_{ij} can be written

$$\chi_i = b_i^{(n)} + \sum_{j\neq i}^N k_c Z_j\left([j|f_i] - [f_i|f_j]\right) \qquad \text{(2-A12)}$$

$$J_{ij} = 2\left[a_i^{(n)} - k_c\left(\frac{\mathrm{erfc}(\alpha R_c)}{2R_c} + \frac{\alpha}{\sqrt{\pi}}\right)\right], i = j \qquad \text{(2-A13a)}$$

$$J_{ij} = k_c\left[[f_i|f_j] - \frac{1}{R_{ij}} + \frac{\mathrm{erfc}(\alpha R_{ij})}{R_{ij}} - \frac{\mathrm{erfc}(\alpha R_c)}{R_c}\right], i \neq j \qquad \text{(2-A13b)}$$

where $[j|f_i]$ and $[f_i|f_j]$ are Coulomb integrals (see B-a) of two atomic densities. According to the Qeq method, the equilibrium charges can be computed by minimizing total electrostatic energy, Eq. (2-A11), under the condition of charge conservation. This is algebraically equivalent to the electronegativity equalization saying that the chemical potentials of each atom, $\mu_i = \frac{\partial E^{\mathrm{ES}}}{\partial q_i}$ be equal to each other: $\mu_1 = \mu_2 = \cdots = \mu_N$. Therefore, the Qeq method leaves N independent equations including the charge conservation condition (usually C=0 with the charge neutrality condition):

$$\sum_i^N q_i = C \qquad \text{(2-A14)}$$

The chemical potentials, the first order partial derivatives of E^{ES} with respect to q_i, are linear functions when the atomic energy term is quadratic. Therefore, the equations for the electronegativity equalization and the charge neutrality condition construct a linear equation

system of N dimension. Rappe and Goddard solve this equation analytically by an inverse matrix method. This method can find an exact solution but can be highly inefficient for systems of large N. Moreover, the coefficient matrix is not symmetric and inverting the matrix can be further inefficient.

The CGM can be more efficient than the matrix method for a large N. However, it can only be used to solve 'unconstrained' optimization problems. Therefore, the equation system should be modified to an unconstrained form to be solved using the CGM method. Our study uses a split-charge equilibration (SQE) method proposed by Nistor et al.[19], which intrinsically allows the charge neutrality condition, and we use the CGM to minimize the total electrostatic energy without any constraint condition. The SQE is based on the principle of Qeq, but is different from the original Qeq in the way of representing atomic charges. This will be explained in more detail in the section d.

As mentioned in the section a, the atomic energy term used in the present study has different expression depending on the range of q_i. Therefore, the coefficients in Eq. (2-A11) should match atomic charges. For a given initial configuration where equilibrium charge values are not assigned to individual atoms, the atomic energy of all atoms can be given as $E_i^{\mathrm{atom}(1)}$ assuming a charge range of [-1e, 1e]. When equilibrium charges for all atoms are computed through the energy minimization process, some atoms may have charge values beyond the initial range. The atomic energy values of those atoms are modified according to the newly computed charge. The subsequent energy minimization using the modified atomic energies may yield new values of equilibrium charges. These minimization processes should be repeated until all the equilibrium charges are in the correct domain of atomic energy. Fortunately, these processes are normally over up to three times and are required only for the initial step where the information on equilibrium charges is not available. Once equilibrium charges are assigned to individual atoms, atomic energy terms for the next step can be directly chosen from the previous ones. The equilibrium charges may change as atomic positions change. However, in ordinary molecular dynamics simulations, the atomic positions of individual atoms do not change abruptly and neither do the equilibrium charges. Therefore, the multiple energy minimization process is not required frequently during a molecular dynamics step except the first time step.

d. Charge representation

In the original Qeq[13], the individual atomic charges are represented by a set of q_i and they are considered as variables to be determined as a solution of an energy minimization problem. In this case, some problematic situations can occur as follows: For example, let's consider an isolated atom from a bulk. If one performs the Qeq with the given configuration, the isolated atom will get some charges even though it must be neutral due to the absence of neighboring atoms to transfer charges around. A similar situation can occur in a simulation containing two different metallic elements. In binary metallic alloys, two metallic atoms would not transfer charges to each other. However, in Qeq simulations, some charges would be given to one type of atoms from the other type of atoms as far as they have different electronegativity. These undesirable situations can be avoided if the atomic charges are generated only when there are neighbor atoms that can accept or donate electrons. Indeed, an ionic bond is formed when the valence electron density between covalently bonded atoms is concentrated on the side of a more electronegative atom.

As one means to describe the formation of ionic bonding more plausibly, Nistor et al.[19] propose a new scheme that allows the charge flow only between covalently bonded neighbors, using the concept of the so-called split-charges. They express the charge q_i of an atom i as

$$q_i = \sum_j^{R_{ij}<R_{ij}^{bond}} \bar{q}_{ji} \qquad \text{(2-A15)}$$

where the split-charge $\bar{q}_{ji}$ represents the charge flow from a covalently bonded neighbor atom j to atom i. R_{ij}^{bond} is the cutoff distance for defining the split-charge, which is sufficiently large so that all first-neighboring atoms with opposite charges are covered. The opposite direction of charge flow is represented by the opposite sign of the split-charge:

$$\bar{q}_{ij} = -\bar{q}_{ji} \qquad \text{(2-A16)}$$

If using the split-charge model, the total electrostatic energy Eq. (2-A11) can be rewritten by substituting Eq. (2-A15)

$$E_{total}^{ES} = \sum_i^N \left[\sum_j^{R_{ij}<R_{ij}^{bond}} \bar{q}_{ji}\right]\chi_i + \frac{1}{2}\sum_{i,j}^N \left[\sum_k^{R_{ik}<R_{ik}^{bond}} \bar{q}_{ki}\right]\left[\sum_l^{R_{lj}<R_{lj}^{bond}} \bar{q}_{lj}\right]J_{ij} \qquad (2\text{-A17})$$

For a given configuration of atoms, we can define all the split-charges by pairing atoms within the cutoff distance, R_{ij}^{bond}, avoiding any duplication from the opposite direction of charge flow. For a system with a total number of bonds *M*, we can generalize Eq. (2-A17) using index of bonds *ab* or *cd* as

$$E_{total}^{ES} = \sum_{ab}^M \bar{q}_{ab}(\chi_b - \chi_a) + \frac{1}{2}\sum_{ab,cd}^M \bar{q}_{ab}\bar{q}_{cd}[(J_{ac} - J_{ad}) - (J_{bc} - J_{bd})] \qquad (2\text{-A18})$$

The coefficient of the first order term in Eq. (2-A18) can be determined by combining $\bar{q}_{ab}$ and $\bar{q}_{ba}$ in Eq. (2-A17). Similarly, the coefficient of the second order term in Eq. (2-A18) is determined by assembling possible combinations of the bond index. We can construct a matrix equation based on Eq. (2-A18),

$$E_{total}^{ES} = \bar{\mathbf{q}}^{\mathbf{T}}\mathbf{b} + \frac{1}{2}\bar{\mathbf{q}}^{\mathbf{T}}\mathbf{A}\bar{\mathbf{q}} \qquad (2\text{-A19})$$

where the *M* dimensional column vectors $\bar{\mathbf{q}}$ and **b** are the set of split-charges and coefficients of the first order term, respectively, and the *M* by *M* symmetric matrix **A** contains coefficients of the second order term. The total electrostatic energy can be minimized by solving the following linear equation:

$$\frac{\partial E_{total}^{ES}}{\partial \bar{\mathbf{q}}} = \mathbf{b} + \mathbf{A}\bar{\mathbf{q}} = \mathbf{0} \qquad (2\text{-A20})$$

using the CGM described in section B-c.

In addition to the concept of the split-charge, Nistor et al.[19] also introduce an additional term to the electrostatic energy using a new binary parameter κ_{ij},

$$E_{total}^{ES} = \sum_i^N q_i\chi_i + \frac{1}{2}\sum_{i,j}^N q_i q_j J_{ij} + \sum_{ij}^M \bar{q}_{ij}^2 \kappa_{ij} \qquad \text{(2-A21)}$$

where κ_{ij} can be interpreted as a bond hardness, in order to improve accuracy of predicting Muliken charges. However, Nistor et al.[19] and Mathieu[20] point out that it can lead to an abrupt change in energy and atomic charges during bond breaking, particularly when interatomic distances are near R^{bond}. Mathieu propose an idea where the split-charge can vanish smoothly as interatomic distances get close to a threshold value (bond breaking limit) by modifying bond hardness κ_{ij} to be dependent on interatomic distances. We, however, determine that this bond hardness term is not essential because the analogous physical meaning is sufficiently included in the presently modified electrostatic energy expression. Moreover, the expense to avoid the discontinuous changes of charge and energy during bond breaking is not trivial. Therefore, in this study, we do not include the bond hardness term but just take the concept of the split-charge.

With this approach, an isolated atom remains neutral because there is no neighbor atom to transfer a charge to. If we do not define the split-charge between metallic elements, no electrostatic interaction exists in purely metallic alloy systems and the systems can be described only by the non-electrostatic term (2NNMEAM formalism, in the present case). In addition, this representation of the atomic charge always ensures charge neutrality of the whole system because the opposite direction of a split-charge has a negative sign. Therefore, the CGM can be applied more straightforwardly and stably. That means that the minimization problem has a symmetric matrix and the numerical errors are not accumulated to the last q variable with no external condition.

D. Mathematical techniques

a. Coulomb integral

The double integral in Eq. (2-A9) with atomic density of Eq. (2-A7) is approximated by Zhou et al.[14] as

$$V_{ij}^{Coul}(q_i, q_j, R_{ij}) = k_c Z_i Z_j \left([f_i|f_j] - [i|f_j] - [j|f_i] + \frac{1}{R_{ij}} \right) + k_c q_i q_j [f_i|f_j] + k_c q_i Z_j ([j|f_i] - [f_i|f_j]) + k_c q_j Z_i ([i|f_j] - [f_i|f_j]) \quad \text{(2-B1)}$$

where notations $[a|f_b]$ and $[f_a|f_b]$ denote the Coulomb interaction integrals:

$$[a|f_b] = \int \frac{f_b(r_b)}{|\mathbf{x}_a - \mathbf{r}_b|} d^3\mathbf{r}_b = \frac{1}{R_{ab}} - \zeta_b \exp(-2\zeta_b R_{ab}) - \frac{1}{R_{ab}} \exp(-2\zeta_b R_{ab}) \quad \text{(2-B2)}$$

$$[f_a|f_b] = \iint \frac{f_a(r_a) f(r_b)}{|\mathbf{r}_a - \mathbf{r}_b|} d^3\mathbf{r}_a d^3\mathbf{r}_b = \frac{1}{R_{ab}} \left[1 - \left(1 + \frac{11}{8}\zeta + \frac{3}{4}\zeta^2 R_{ab}^2 + \frac{1}{6}\zeta^3 R_{ab}^3 \right) \exp(-2\zeta R_{ab}) \right] \text{ for } \zeta_a = \zeta_b = \zeta \quad \text{(2-B3a)}$$

$$[f_a|f_b] = \frac{1}{\mathrm{R_{ab}}} - \frac{\zeta_a \zeta_b^4 \exp(-2\zeta_a R_{ab})}{(\zeta_a + \zeta_b)^2 (\zeta_a - \zeta_b)^2} - \frac{\zeta_b \zeta_a^4 \exp(-2\zeta_b R_{ab})}{(\zeta_b + \zeta_a)^2 (\zeta_b - \zeta_a)^2} - \frac{(3\zeta_a^2 \zeta_b^4 - \zeta_b^6) \exp(-2\zeta_a R_{ab})}{R_{ab} (\zeta_a + \zeta_b)^3 (\zeta_a - \zeta_b)^3} - \frac{(3\zeta_b^2 \zeta_a^4 - \zeta_a^6) \exp(-2\zeta_b R_{ab})}{R_{ab} (\zeta_b + \zeta_a)^3 (\zeta_b - \zeta_a)^3} \text{ for } \zeta_a \neq \zeta_b \quad \text{(2-B3b)}$$

The first term of Eq. (2-B1) is independent from atomic charges; therefore, it can be regarded as a non-electrostatic term. In the present study, this term is merely neglected as in the studies of Streitz and Mintmire[16], and Zhou et al.[14]

b. Charge-neutralized real-space direct summation method

The Coulomb potential decays inversely with the distance R_{ij} between two point charges i and j, so that it has an infinite effective range. Furthermore, the total Coulomb energy of N ions which is expressed by the sum of all pair interactions including infinitely repeated periodic images as

$$E_{total}^{Coul} = \frac{1}{2}\sum_{i=1}^{N}\sum_{j\neq i}^{\infty}\frac{q_i q_j}{R_{ij}} \qquad \text{(2-B4)}$$

has an intrinsic convergence problem. In the practical molecular dynamics simulations, interatomic potential should be effectively cut off within a proper distance. However, when the long-range Coulomb potential is cut off using an ordinary method, it causes significant errors and artifacts. Classically, the Ewald method[17] has been used in the simulation of ionic materials systems. In the Ewald method, the total electrostatic interaction energy is divided into two parts: a short-range and a long-range contribution. Mathematically, these two parts can be divided by using a simple trick replacing unity with the sum of error-function (erf) and complementary error-function (erfc = 1 − erf), that is

$$E_{total}^{Coul} = \frac{1}{2}\sum_{i=1}^{N}\sum_{j\neq i}^{\infty}\frac{q_i q_j}{R_{ij}}\left[\mathrm{erfc}\left(\alpha R_{ij}\right) + \mathrm{erf}(\alpha R_{ij})\right] \qquad \text{(2-B5)}$$

The erfc(αR_{ij}) term in Eq. (2-B5) is rapidly converged at short-range distance so that can be dealt with real-space direct summation, and the long-range contribution of erf(αR_{ij}) term is evaluated by taking the Fourier transform to reciprocal-space. This Ewald method can evaluate the Coulomb potential energy with a high accuracy; however the computational cost is rather expensive due to the Fourier transform.

Wolf et al.[18] suggested a novel summation method for the Coulomb pairwise potential in ionic systems without using the Fourier transform, resulting in higher computation efficiency than the Ewald method. The basic concept of the Wolf method comes from the fact that the errors from real-space direct summation are dramatically reduced when a spherically truncated

group summed over is electrically neutral. However, the evaluation of total Coulomb energy with only this charge neutralized truncation method still has non-negligible errors depending on the cutoff distance, R_c. Therefore, Wolf and coworkers use a damped Coulomb pair potential using a complementary error-function so as to more rapidly converge with increasing cutoff distance. Finally, the total Coulomb potential energy can be evaluated using the Wolf method by Eq. (2-B6).

$$\frac{1}{2}\sum_{i=1}^{N}\sum_{j\neq i}^{\infty}\frac{q_i q_j}{R_{ij}} \approx \frac{1}{2}\sum_{i=1}^{N}\sum_{j(i\neq j)}^{R_{ij}<R_c} q_i q_j\left(\frac{\mathrm{erfc}(\alpha R_{ij})}{R_{ij}} - \lim_{R_{ij}\to R_c}\frac{\mathrm{erfc}(\alpha R_{ij})}{R_{ij}}\right) - \sum_{i}^{N} q_i^2\left(\frac{\mathrm{erfc}(\alpha R_c)}{2R_c} + \frac{\alpha}{\sqrt{\pi}}\right) \tag{2-B6}$$

Here, α is a damping parameter which controls the balance between convergence speed and accuracy. The first term on the right hand side of Eq. (2-B6) is a representation of damped Coulomb pair potential and, the second and third terms guarantee the charge neutrality of all atoms in the cutoff sphere. The last term is the self-energy term that uses the $R_{ij}\to 0$ limit of the erf term in Eq. (2-B5) instead of performing the full Fourier transform. Using this approach, it is possible to accurately reproduce the total Coulomb interaction energy of ionic systems.

c. Conjugate gradient method

An N dimension linear equation system

$$\mathbf{Ax} = \mathbf{b} \tag{2-B7}$$

for a vector **x** where the matrix **A** is known, symmetric, positive definite, and real, and vector **b** is also known, can be solved by a conjugate gradient method (CGM) which finds a numerical solution with iterative algorithm. At the beginning, initial guessed solution $\mathbf{x}_0$ is given (usually, $\mathbf{x}_0=\mathbf{0}$) and the next optimal solution for **x** can be determined as

$$\mathbf{x}_{k+1} = \mathbf{x}_k + \alpha_k \mathbf{d}_k \tag{2-B8}$$

using a march distance α_k and a search direction $\mathbf{d}_k$. This procedure makes residual vector $\mathbf{r}_k$, Eq. (2-B9), close to the zero vector.

$$\mathbf{r}_k = \mathbf{b} - \mathbf{A}\mathbf{x}_k \qquad \text{(2-B9)}$$

In order to reach $\mathbf{r}_k \rightarrow \mathbf{0}$ stably and efficiently, the CGM uses conjugate gradient vectors for search directions which satisfy,

$$\mathbf{d}_i^{\mathbf{T}}\mathbf{A}\mathbf{d}_j = 0 \qquad \text{(2-B10)}$$

Here, $i \neq j$ and $\mathbf{d}$ is non-zero. The detailed algorithm for solving Eq. (2-B7) by the CGM is summarized as follows:

(1) Set initial vectors $\mathbf{x}_0=\mathbf{0}$, $\mathbf{r}_0$ by Eq. (2-B9) and $\mathbf{d}_0=\mathbf{r}_0$.

(2) Compute the march distance, $\alpha_k = \frac{\mathbf{r}_k^{\mathbf{T}}\mathbf{r}_k}{\mathbf{d}_k^{\mathbf{T}}\mathbf{A}\mathbf{d}_k}$ (for k=0, 1, 2, …), the next optimal solution, $\mathbf{x}_{k+1}$, by Eq. (2-B10) and the residual vector, $\mathbf{r}_{k+1} = \mathbf{r}_k - \alpha_k\mathbf{A}\mathbf{d}_k$. If all elements of the residual vector are sufficiently small, then $\mathbf{x}_{k+1}$ at this iteration would be the solution.

(3) If not, the new iteration is continued with a new search direction, $\mathbf{d}_{k+1} = \mathbf{r}_{k+1} + \frac{\mathbf{r}_{k+1}^{\mathbf{T}}\mathbf{r}_{k+1}}{\mathbf{r}_k\mathbf{r}_k}\mathbf{d}_k$ until the residual vector is close to zero.

3. Evaluation of developed potentials for binary systems (Li-Mn, Li-O and Mn-O)

A. Equation of state curve for B2-LiMn

In case of the Li-Mn binary system, there is no stable compound to be considered for parameter optimization. Therefore, we first determine the E_c, R_e, α, d_{rep} and d_{att} parameters of the Li-Mn pair by fitting the equation of state (EOS) for a given reference structure (B2 in this study) to DFT calculation. The EOS curves calculated from our potential and from the DFT are shown in figure on the right.

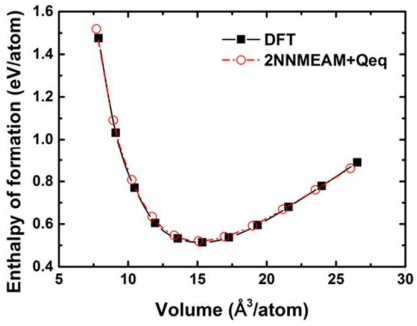

B. Properties of lithium oxide compounds

The Li-O binary phase diagram[21] shows two stable oxide phases: anti-fluorite type Li_2O (space group: $Fm\bar{3}m$[22]) and lithium peroxide Li_2O_2 (space group: $P63/mmc$[23]). There also exists a high-pressure phase of Li_2O, reported by Lazicki et al.[24], who observed a reversible phase change from the cubic anti-fluorite (α) to orthorhombic anti-cotunnite type (β, space group: *Pnma*) phase at 50 GPa and ambient temperatures. Crystal structures these three phases are represented in the following figures.

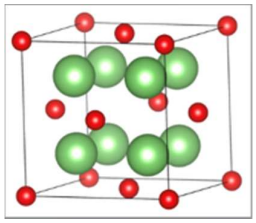
α-Li_2O

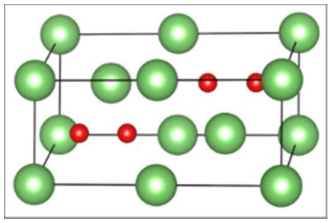
Li_2O_2

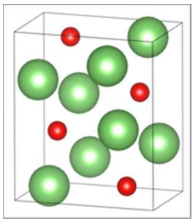
β-Li_2O_2

To evaluate whether the developed potential can reproduce the structural properties of lithium oxide compounds, we compare the calculated lattice parameters of α-Li_2O, β-Li_2O and Li_2O_2 phases with experimental data and DFT calculations in the following table. The relative error of our calculation for the lattice parameter of α-Li_2O is about 1% when compared to the experimental data[22], and our calculation is also close to the DFT calculation[25]. We calculate the lattice parameters of β-Li_2O at high pressure (61.9 GPa) as well as ambient pressure for direct

comparison with the experimental data[24] observed at high pressure (61.9 GPa). Our calculation is close to the DFT calculation at ambient pressure[25], but generates relatively higher error with respect to the experimental data at high pressure. The calculated lattice parameter of Li_2O_2 is within an acceptable error range from experimental data[23].

Phase		2NNMEAM+Qeq	% error	Expt.	DFT [d]	% error
α-Li_2O	*a* (Å)	4.6599	+1.08	4.61 [a]	4.659	+1.06
β-Li_2O	*a* (Å)	5.3343 / 4.8005 [*]	+7.73	4.456 [*,b]	5.152	
(0 pressure / 61.9 GPa)	*b* (Å)	3.2478 / 3.2063 [*]	+15.07	2.7865 [*,b]	3.14	
	c (Å)	5.8938 / 4.9524 [*]	-4.98	5.212 [*,b]	5.933	
Li_2O_2	*a* (Å)	2.9031	-7.60	3.142 [c]	3.18	+1.21
	c (Å)	8.2524	+7.87	7.65 [c]	7.704	+0.71
rRMSE (%)			7.40			0.87

[*] at 61.9 GPa, [a] Ref. [22], [b] Ref. [24], [c] Ref. [23], [d] Ref. [25]

	2NNMEAM +Qeq	Expt.	DFT
		α-Li_2O	
B	118	88 [a]	79,[c] 94 [d]
C_{11}	271	217 [a]	198,[c] 237 [d]
C_{12}	42	25 [a]	19,[c] 28 [d]
C_{44}	61	68 [a]	57,[c] 68 [d]
		β-Li_2O	
B	101	188 [*,b]	80 [e]
		Li_2O_2	
B	195		73,[c] 98 [f]

[*] at 61.9 GPa, [a] Ref. [26], [b] Ref. [24], [c] Ref. [25], [d] Ref. [27], [e] Ref. [28], [f] Ref. [29]

Table on the left shows the calculated elastic constants of three lithium oxide phases in comparison with the experimental data[24,26] and DFT calculations[25,27–29]. The calculated elastic constants of α-Li_2O agree well with both the experimental data and DFT calculations. The bulk modulus of β-Li_2O matches with the DFT calculation rather than with the experimental data at high pressure, while that of Li_2O_2 overestimates the DFT calculation.

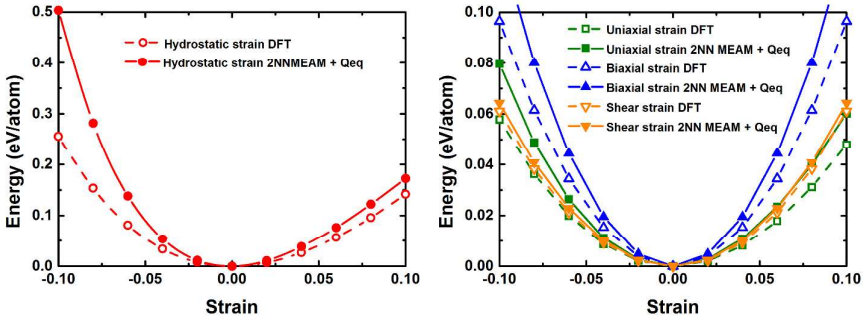

This figure shows the equation of state of α-Li_2O under hydrostatic, uniaxial, biaxial and shear strain, calculated using the potential in comparison with DFT calculation also performed

in the present work. The average equilibrium charges assigned to Li and O atoms for α(β)-Li_2O are +0.356 (+0.349) and -0.712 (-0.698) e, and for Li_2O_2 are +0.433 and -0.433 e, respectively. We do not consider the charge states of individual elements as a target property of fitting, but obtain them as a result of the fitting to better reproduce other properties and to make the simulation stable. Too large charge values often cause the instability problem during the simulation.

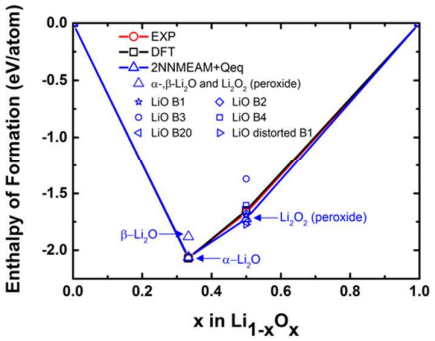

To verify that our potential can correctly reproduce the energetics of lithium oxide phases, we compare the calculated enthalpy of formation, ΔH_f, with experimental data[21] and DFT calculation[25] in figure on the left. The reference state is bcc Li and O_2 gas.

The calculated ΔH_f of α-Li_2O and Li_2O_2 (peroxide) agree well with the experimental data and the DFT calculation. β-Li_2O is an unstable phase at ambient pressure and is expected to have a higher value of ΔH_f than α-Li_2O, which is reproduced well by the present calculation. We also calculate ΔH_f of other hypothetical LiO phases such as B1, B2, B3, B4, B20 and distorted B1 structures to check whether the potential reproduces a wrong phase as the stable phase. Those phases are not stable compounds; therefore, the ΔH_f of those phases should be above the convex hull of the ΔH_f curve. However, according to the present calculation, LiO phases of B20 and distorted B1 have lower energy than that of the experimentally stable Li_2O_2 (peroxide) phase. Although this is not desirable, we had to accept it because it was not trivial to correct this without compromising the reproducibility for the structural and elastic properties of Li_2O and Li_2O_2 phases. More details on this are discussed later in this section.

One of the most important properties of LIB cathode materials is the lithium diffusion properties. We calculate the lithium migration energy barrier in α-Li_2O and compare with reference data to ensure the reliability of the potential in reproducing the diffusion properties. To calculate the lithium migration energy barrier, one vacancy site is generated by removing one lithium atom, and the relative energy difference is calculated as a neighboring lithium atom migrates to the vacancy site along a linear path. The energy of each sample is calculated by completely equilibrating the cell size and the position of all other atoms except the migrating atom.

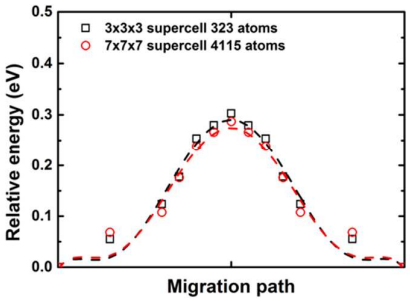

To check the cell size effect in the calculation, we carry out the calculation for various cell sizes from 3×3×3 (323 atoms) to 7×7×7 (4115 atoms) super cells, and confirm that the size effect can be ignored, as shown in figure on the left. The calculated lithium migration energy barrier in α-Li_2O, around 0.3 eV, matches well with the experimental data, 0.49[30] and 0.31 eV[31], and DFT calculations, 0.34[32], 0.30[33], 0.29[34] and 0.28-0.33 eV[35].

According to our experience, so many potentials that perform well at 0 K often fail at finite temperatures. The representative example of this failure is a transformation of the structure into an unknown structure, with a decrease in the energy to a level that makes the unknown structure a stable phase on the phase diagram. In this case, one cannot use the potential for finite temperature simulations at least at the relevant compositional region. To check the applicability of the potential for finite temperature simulations, we examine the energy and structural changes of all compound phases considered during heating and after cooling. The initial structure of each compound phase relaxed at 0 K is heated to 3000 K, increasing the temperature by 200 K and equilibrating the structure (containing 2000-4000 atoms) for 10 ps at each temperature with a Parrinello-Rahman *NpT* ensemble. Then, the structure heated to each temperature and rapidly cooled to 0 K is examined to determine whether the initial structure and energy have been recovered. From the recovery of the initial (0 K) structure and energy after rapid cooling, one can confirm that the potential does not generate undesirable structural changes during dynamic simulations (at finite temperatures).

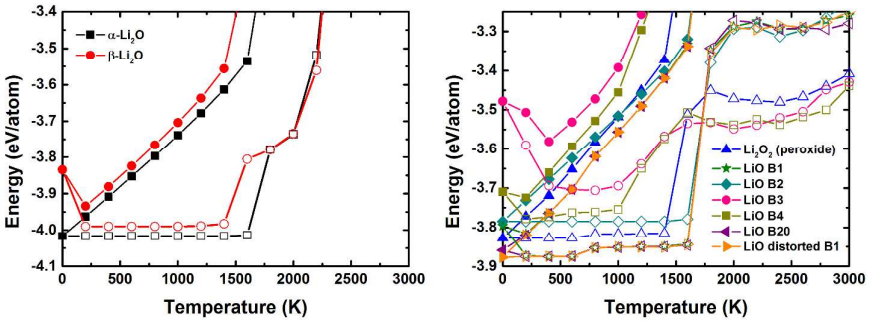

This figure shows the change in internal energy of the lithium oxide phases, obtained from the above-described simulation as a function of temperature. The solid symbols represent the

energy during heating; the open symbols represent the energy after rapid cooling to 0 K from each temperature. The experimentally stable lithium oxide phases (α-Li_2O and Li_2O_2 peroxide) exhibit a monotonic increase in energy as the temperature increases and recover the initial 0 K energy after rapid cooling, which is a desirable result. Although some transformations involving a decrease in energy occur in the metastable β-Li_2O phase and hypothetical B3 and B4 phases of LiO, these are not problematic because the decrease in the energy does not exceed the criterion that a wrong phase should not be the most stable phase at the corresponding composition. However, it should be noted that the hypothetical LiO B1 and B20 phases transform to a distorted B1 structure with a decrease in energy and have an energy lower than that of the experimentally stable Li_2O_2 (peroxide) phase by 0.049 eV/atom. This means that the present potential predicts this distorted B1 structure as the most stable phase, in contrast to experiments, at the equiatomic composition. We finally decided to accept this flaw in our potential, because this flaw was difficult to remove while maintaining the good performance of the potential obtained for other properties and it was found later on that the flaw does not cause a serious fault in the stability of ternary Li-Mn-O compounds. However, careful attention should be paid to the phase stability when using the present potential for an MD simulation near the equiatomic composition (x_O = 0.5) of the binary Li-O system. We think this flaw originates from the potential formalism rather than selection of parameter set, but have not found the exact reason. We will try to clarify the exact reason of this problem continuously in the further work.

C. Properties of manganese oxide compounds

The Mn-O system contains the phases manganosite ($Mn_{1-x}O$, space group: $Fm\bar{3}m$), α-hausmannite (α-Mn_3O_4, space group: $I4_1/amd$), which transforms to β-Mn_3O_4 (space group: $Fd\bar{3}m$) at high temperatures (> 1450 K) (distorted tetragonal structure to cubic structure), β-bixbyite (β-Mn_2O_3, space group: $Ia\bar{3}$), which transforms to α-Mn_2O_3 (space group: *Pbca*) at temperatures below 300 K and pyrolusite (β-MnO_2, space group: $P4_2/mnm$)[36]. There are several metastable phases of MnO_2: cryptomelane (α, space group: $I4/m$), ramsdellite (γ, space group: *Pnma*) and defective spinel MnO_2 (λ, space group: $Fd\bar{3}m$). In this study, we consider all the phases listed above except for α-Mn_2O_3 and α-Mn_3O_4. Since the tetragonal structure of α-Mn_2O_3 is not much different from the cubic β-Mn_2O_3 structure, only the cubic β-Mn_2O_3 is considered. The distorted structure of α-Mn_3O_4 is known to be generated by Jahn-Teller distortion[36]. However, the present potential cannot reproduce such distortion, and this structure is not considered any more in the present work. $Mn_{1-x}O$ manganosite is known to have intrinsic cation vacancies in the lattice, and the γ-MnO_2 phase consists of an intergrowth of pyrolusite and the ramsdellite structure. For simplicity, manganosite is regarded as perfect MnO and γ-MnO_2 as pure ramsdellite in the present study. In addition to those phases, the metastable monoclinic Mn_5O_8 (space group: $C2/m$) phase is also considered. Crystal structures of manganese oxide phases are represented in the following figures.

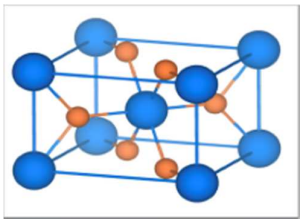

MnO_2 pyrolusite

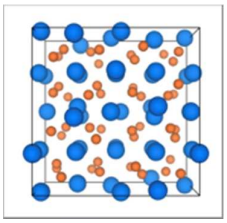

Mn_2O_3 bixbyte

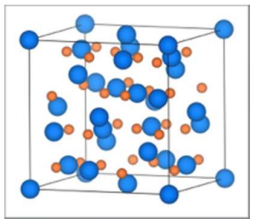

Mn_3O_4 hausmanite

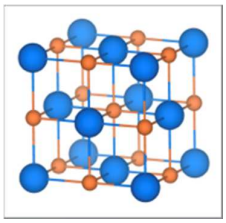

MnO manganosite

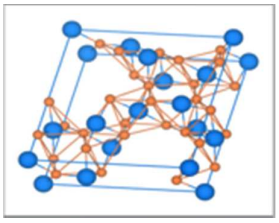

MnO_2 cryptomelane

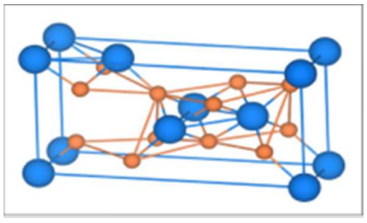

MnO_2 ramsdellite

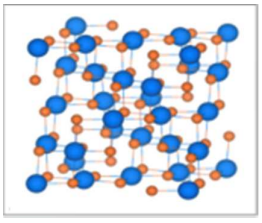

λ-MnO_2

For the same purpose as in the Li-O binary system, we compare the fundamental materials properties (lattice parameters, elastic constants and enthalpy of formation) of manganese oxide phases calculated using the developed Mn-O binary potential with experimental data and/or DFT calculations. We also check the reliability of the potential at finite temperatures.

This table shows the calculated lattice parameters of the manganese oxide phases in comparison with experimental data[37–44] and DFT calculation[25]. The relative root mean-squared error (rRMSE) of the present calculation is 4.37% with respect to the experimental data.

Phase		2NNMEAM+Qe	% error	Expt.	DFT [1]	% error
α-MnO_2	*a* (Å)	9.9204	+1.36	9.7876 [a]	9.924	+1.39
	c (Å)	2.9032	+1.33	2.8650 [a]	2.929	+2.23
β-MnO_2	*a* (Å)	4.5003	+2.26	4.4008 [b]	4.452	+1.16
	c (Å)	2.8773	+0.10	2.8745 [b]	2.939	+2.24
γ-MnO_2	*a* (Å)	9.3190	+0.49	9.2734 [c]	9.396	+1.32
	b (Å)	2.9058	+1.47	2.8638 [c]	2.932	+2.38
	c (Å)	4.7344	+4.70	4.5219 [c]	4.646	+2.74
λ-MnO_2	*a* (Å)	8.2503	+2.56	8.0445 [d]	8.247	+2.52
Mn_5O_8	*a* (Å)	10.1228	-2.17	10.347 [f]	10.484	+1.32
	b (Å)	5.5079	-3.78	5.724 [f]	5.862	+2.41
	c (Å)	4.7192	-2.74	4.852 [f]	4.978	+2.60
	β (°)	109.7470	+0.31	109.41 [f]	109.29	-0.11
β-Mn_2O_3	*a* (Å)	9.0940	-3.40	9.414 [e]	9.616	+2.15
β-Mn_3O_4	*a* (Å)	8.1121	-5.01	8.54 [g]		
MnO	*a* (Å)	4.0239	-9.43	4.44 [h]	4.495	+1.17
rRMSE (%)			4.37			1.92

[a] Ref. [37], [b] Ref. [38], [c] Ref. [39], [d] Ref. [40], [e] Ref. [42], [f] Ref. [41], [g] Ref. [43], [h] Ref. [44], [1] Ref. [25]

phase	2NNMEAM+Qe	DFT [a]
α-MnO_2	63	107
β-MnO_2	119	173
γ-MnO_2	92	103
λ-MnO_2	54	87
Mn_5O_8	134	136
β-Mn_2O_3	143	150
β-Mn_3O_4	138	
MnO	167	143

[a] Ref. [25]

Table on the left summarizes the calculated bulk modulus of the manganese oxide phases together with DFT calculation[25]. The present potential generally underestimates the bulk modulus of the MnO_2 phases compared to the DFT calculation, while overestimating the bulk modulus of MnO manganosite. The agreement for the other phases is good.

	2NNMEAM+Qeq	Expt [a]	DFT [b]	DFT [c]
B	167	154	143	170
C_{11}	358	223	209	281
C_{12}	70	120	110	166
C_{44}	48	79	77	96

[a] Ref. [45], [b] Ref. [25], [c] Ref. [46]

Table on the left shows our calculation for the elastic constants of MnO in comparison with experimental data[45] and DFT calculations[25,46]. The calculated elastic constants are in reasonable agreement with the reference.

The calculated equilibrium charges of the Mn ion are +0.93, +0.89, +0.86 and +0.78 e for MnO_2, Mn_2O_3, Mn_3O_4 and MnO, respectively. The Bader charges of Mn by DFT+*U* calculation[47] are +2.09, +1.95 and +1.65 for MnO_2, Mn_2O_3 and MnO, respectively. The present potential shows the same tendency as that of the DFT calculation for the charge states in various stoichiometry, although it underestimates the absolute value. It should be noted here that the atomic charge is not a well-defined quantity even in DFT calculations.

Figure on the right shows the calculated enthalpy of formation, ΔH_f, of manganese oxide phases with experimental data[36] and DFT calculation[25]. The reference state is α-Mn and O_2 gas. The results are in excellent agreement with both the experimental data and the DFT calculation.

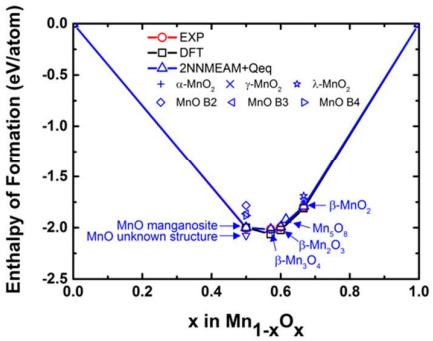

In the case of the MnO_2 phases, there are several polymorphs in addition to the stable β phase. The present potential reproduces β-MnO_2 as the most stable phase, which is consistent with the experiment. The energy differences from β-MnO_2 are predicted to be 0.043, 0.044 and 0.103 eV/atom for the α, γ and λ phases, respectively. However, it should be noted that the present potential predicts an unknown structure of MnO as a more stable phase than manganosite, the experimentally known stable phase at this composition, similar to the case in the Li-O system.

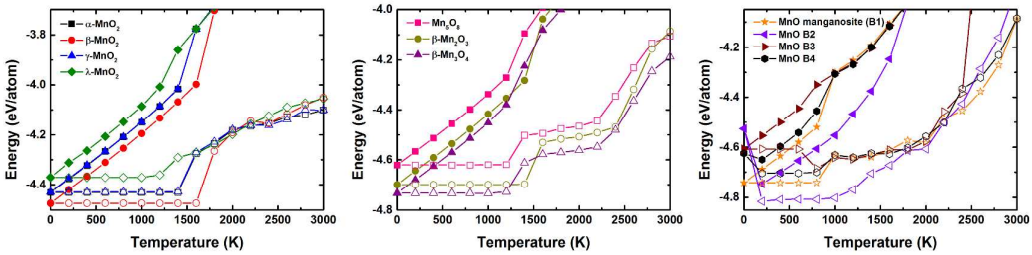

This figure shows the change in internal energy of manganese oxide phases with temperature, obtained from the same MD simulations described above. The energy levels of all the MnO_2, Mn_5O_8, Mn_2O_3, and Mn_3O_4 phases monotonically increase as the temperature increases and recover to 0 K energy after rapid cooling. From this, we confirm that the present Mn-O binary potential does not generate undesirable structure changes for MnO_2, Mn_5O_8, Mn_2O_3 and M_3O_4 phases during dynamic simulations at finite temperatures. However, there are some structural changes, accompanied by a

decrease in energy during MD simulations at equiatomic composition. Hypothetical MnO phases of the B2, B3 and B4 structures transform to unknown structures with a decrease in energy, as shown in the figure. The B3 and B4 phases are not problematic since the transformed structure has a higher energy than that of manganosite. The problem is that the energy of unknown structure transformed from the B2 phase is lower than that of manganosite by 0.08 eV/atom. Although this is undesirable, it is also difficult to remove this flaw, similarly to the case of the Li-O system. Careful attention should be paid to the phase stability when using the present potential for MD simulations near the equiatomic composition ($x_O = 0.5$) of the binary Mn-O system.

Despite sufficient parameter optimization, the reproducibility of some structures is unsatisfactory. We believe that the origin of the disagreement is absolutely the potential formalism. It is widely accepted that no (semi-)empirical potential formalism can be perfect. The more sophisticated the formalism is, the better and wider the applicability of the potential is. However, the portion of the potential parameter cannot be excluded completely. This is the first ternary potential we developed using the recently developed 2NNMEAM+Qeq formalism. We will continuously make an effort to find more complete parameter optimization procedure and to improve the formalism for better descriptions of materials system. What we can do at this moment with the already developed potentials is to pay attention to the completeness of the potential when analyzing the simulation results, distinguishing the physically meaningful results and probable artifacts that may come from the incompleteness of the potential. The developed potentials reproduce the fundamental physical properties of important compounds of Li-Mn, Li-O, Mn-O satisfactorily well and do not cause serious artifacts during simulation. Therefore, they have a sufficiently good performance to extend to ternary Li-Mn-O potential.

The followings are crystal structures of the ternary lithium manganese oxides considered in the present study.

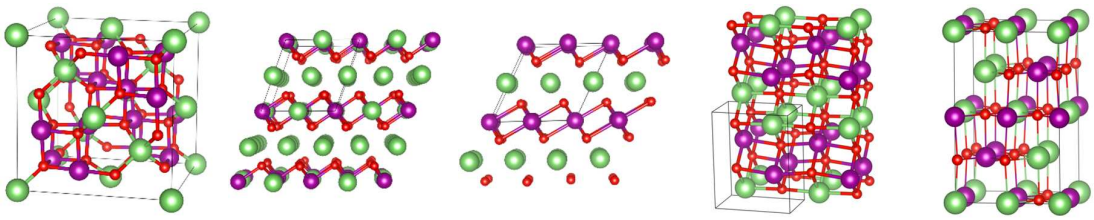

spinel $LiMn_2O_4$ layered Li_2MnO_3 layered $LiMnO_2$ *o*-$LiMnO_2$ *t*-$LiMnO_2$

REFERENCES

(1) Rose, J. H.; Smith, J. R.; Guinea, F.; Ferrante, J. Universal Features of the Equation of State of Metals. *Phys. Rev. B* **1984**, *29*, 2963–2969.

(2) Baskes, M. I. Modified Embedded-Atom Potentials for Cubic Materials and Impurities. *Phys. Rev. B* **1992**, *46*, 2727–2742.

(3) Baskes, M. I. Determination of Modified Embedded Atom Method Parameters for Nickel. *Mater. Chem. Phys.* **1997**, *50*, 152–158.

(4) Lee, B.-J.; Baskes, M. I. Second Nearest-Neighbor Modified Embedded-Atom-Method Potential. *Phys. Rev. B* **2000**, *62*, 8564–8567.

(5) Lee, B.-J.; Baskes, M. I.; Kim, H.; Cho, Y. K. Second Nearest-Neighbor Modified Embedded Atom Method Potentials for Bcc Transition Metals. *Phys. Rev. B* **2001**, *64*, 184102 1-11.

(6) Lee, B.-J.; Shim, J.-H.; Baskes, M. I. Semiempirical Atomic Potentials for the Fcc Metals Cu, Ag, Au, Ni, Pd, Pt, Al, and Pb Based on First and Second Nearest-Neighbor Modified Embedded Atom Method. *Phys. Rev. B* **2003**, *68*, 144112 1-11.

(7) Lee, B.-J.; Ko, W.-S.; Kim, H.-K.; Kim, E.-H. The Modified Embedded-Atom Method Interatomic Potentials and Recent Progress in Atomistic Simulations. *Calphad* **2010**, *34*, 510–522.

(8) Kim, Y.-K.; Jung, W.-S.; Lee, B.-J. Modified Embedded-Atom Method Interatoic Potentials for the Ni-Co Binary and the Ni-Al-Co Ternary Systems. *Model. Simul. Mater. Sci. Eng.* **2015**, *23*, 55004 1-18.

(9) Kim, H.-K.; Jung, W.-S.; Lee, B.-J. Modified Embedded-Atom Method Interatomic Potentials for the Nb-C, Nb-N, Fe-Nb-C, and Fe-Nb-N Systems. *J. Mater. Res.* **2010**, *25*, 1288–1297.

(10) Vinet, P.; Ferrante, J.; Smith, J. R.; Rose, J. H. A Universal Equation of State for Solids. *J. Phys. C Solid State Phys.* **1986**, *19*, L467–L473.

(11) Smith, J. R.; Schlosser, H.; Leaf, W.; Ferrante, J.; Rose, J. H. Connection between Energy Relations of Solids and Molecules. *Phys. Rev. A* **1989**, *39*, 514–517.

(12) Ferrante, J.; Schlosser, H.; Smith, J. R. Global Expression for Representing Diatomic Potential-Energy Curves. *Phys. Rev. A* **1991**, *43*, 3487–3494.

(13) Rappe, A. K.; Goddard III, W. A. Charge Equilibration for Molecular Dynamics Simulations. *J. Phys. Chem.* **1991**, *95*, 3358–3363.

(14) Zhou, X. W.; Wadley, H. N. G.; Filhol, J.-S.; Neurock, M. N. Modified Charge Transfer–embedded Atom Method Potential for Metal/metal Oxide Systems. *Phys. Rev. B* **2004**, *69*, 035402 1-20.

(15) Liang, T.; Devine, B.; Phillpot, S. R.; Sinnott, S. B. Variable Charge Reactive Potential for Hydrocarbons to Simulate Organic-Copper Interactions. *J. Phys. Chem. A* **2012**, *116*, 7976–7991.

(16) Streitz, F. H.; Mintmire, J. W. Electrostatic Potential for Metal-Oxide Surfaces and Interfaces. *Phys. Rev. B* **1994**, *50*, 11996–12003.

(17) Parry, D. E. The Electrostatic Potential in The Surface Region of an Ionic Crystal. *Surf. Sci.* **1975**, *49*, 433–440.

(18) Wolf, D.; Keblinski, P.; Phillpot, S. R.; Eggebrecht, J. Exact Method for the Simulation of Coulombic Systems by Spherically Truncated, Pairwise R-1 Summation. *J. Chem. Phys.* **1999**, *110*, 8254–8282.

(19) Nistor, R. A.; Polihronov, J. G.; Müser, M. H.; Mosey, N. J. A Generalization of the Charge Equilibration Method for Nonmetallic Materials. *J. Chem. Phys.* **2006**, *125*, 094108 1-10.

(20) Mathieu, D. Split Charge Equilibration Method with Correct Dissociation Limits. *J. Chem. Phys.* **2007**, *127*, 224103 1-12.

(21) Chang, K.; Hallstedt, B. Thermodynamic Assessment of the Li–O System. *Calphad* **2011**, *35*, 160–164.

(22) Farley, T.; Hayes, W. Investigation of Thermally Induced Li^+ Ion Disorder in Li_2O Using Neutron Diffraction. *J. Phys. Condens. Matter* **1991**, *3*, 4761–4781.

(23) Cota, L. G.; de la Mora, P. On the Structure of Lithium Peroxide, Li_2O_2. *Acta Crystallogr.* **2005**, *B61*, 133–136.

(24) Lazicki, A.; Yoo, C.-S.; Evans, W. J.; Pickett, W. E. Pressure-Induced Antifluorite-to-Anticotunnite Phase Transition in Lithium Oxide. *Phys. Rev. B* **2006**, *73*, 184120 1-7.

(25) Jain, A.; Ong, S. P.; Hautier, G.; Chen, W.; Richards, W. D.; Dacek, S.; Cholia, S.; Gunter, D.; Skinner, D.; Ceder, G.; et al. Commentary: The Materials Project: A Materials Genome Approach to Accelerating Materials Innovation. *APL Mater.* **2013**, *1*, 011002 1-11.

(26) Hull, S.; Farley, T. W. D.; Hayes, W.; Hutchings, M. T. The Elastic Properties of Lithium Oxide and Their Variation with Temperature. *J. Nucl. Mater.* **1988**, *160*, 125–134.

(27) Li, X.-F.; Chen, X.-R.; Meng, C.-M.; Ji, G.-F. Ab Initio Calculations of Elastic Constants and Thermodynamic Properties of Li_2O for High Temperatures and Pressures. *Solid State Commun.* **2006**, *139*, 197–200.

(28) Kunc, K.; Loa, I.; Grzechnik, A.; Syassen, K. Li_2O at High Pressures: Structural Properties, Phase-Transition, and Phonons. *Phys. Status Solidi B* **2005**, *242*, 1857–1863.

(29) Wu, H.; Zhang, H.; Cheng, X.; Cai, L. Ab Initio Calculations of Structural, Elastic and Electronic Properties of Li_2O_2. *Philos. Mag.* **2007**, *87*, 3373–3383.

(30) Chadwick, A. V.; Flack, K. W.; Strance, J. H.; Harding, J. Defect Structures and Ionic Transport in Lithium Oxide. *Solid State Ionics* **1988**, *28–30*, 185–188.

(31) Heitjans, P.; Indris, S. Diffusion and Ionic Conduction in Nanocrystalline Ceramics. *J. Phys. Condens. Matter* **2003**, *15*, R1257–R1289.

(32) De Viat, A.; Gillan, M. J.; Lin, J. S.; Payne, M. C.; Stich, I.; Clarke, L. J. Defect Energetic in Oxide Materials from First Principles. *Phys. Rev. Lett.* **1992**, *68*, 3319–3322.

(33) Koyama, Y.; Yamada, Y.; Tanaka, I.; Nishitani, S. R.; Adachi, H.; Murayama, M.; Kanno, R. Evaluation of Migraion Energy of Lithium Ions in Chalcogenides and Halides by First Principles Calculations. *Mater. Trans.* **2002**, *43*, 1460–1463.

(34) Hayoun, M.; Meyer, M.; Denieport, A. Complex Atomic-Diffusion Mechanism in Ionic Superconductors: The Case of the Lithium-Oxide Antifluorite. *Acta Mater.* **2005**, *53*, 2867–2874.

(35) Islam, M. M.; Bredow, T.; Minot, C. Theoretical Analysis of Structural, Energetic, Electronic, and Defect Properties of Li_2O. *J. Phys. Chem. B* **2006**, *110*, 9413–9420.

(36) Grundy, A. N.; Hallstedt, B.; Gauckler, L. J. Assessment of the Mn-O System. *J. Phase Equilibria* **2003**, *24*, 21–39.

(37) Rossouw, M.; Liles, D.; Thackeray, M.; David, W.; Hull, S. Alpha Manganese Dioxide for Lithium Batteries: A Structural and Electrochemical Study. *Mater. Res. Bull.* **1992**, *27*, 221–230.

(38) Haines, J.; Léger, J. M.; Hoyau, S. Second-Order Rutile-Type to $CaCl_2$-Type Phase Transition in β-MnO_2 at High Pressure. *J. Phys. Chem. Solids* **1995**, *56*, 965–973.

(39) Post, J. E.; Heaney, P. Neutron and Synchrotron X-Ray Diffraction Study of the Structures and Dehydration Behaviors of Ramsdellite And “groutellite.” *Am. Mineral.* **2004**, *89*, 969–975.

(40) Thackeray, M. M.; de Kock, A.; David, W. I. F. Synthesis and Structural Characterization of Defect Spinels in the Lithium-Manganese-Oxide System. *Mater. Res. Bull.* **1993**, *28*, 1041–1049.

(41) Oswald, H. R.; Wampetich, M. J. Die Kristallstrukturen von Mn_5O_8 Und $Cd_2Mn_3O_8$. *Helv. Chim. Acta* **1967**, *50*, 2023–2034.

(42) Geller, S.; Espinosa, G. P. Magnetic and Crystallographic Transitions in Sc^{3+}, Cr^{3+}, and Ga^{3+} Substituted Mn_2O_3. *Phys. Rev. B* **1970**, *1*, 3763–3769.

(43) van Hook, H. J.; Keith, M. L. The System Fe_3O_4-Mn_3O_4. *Am. Mineral.* **1958**, *43*, 69–83.

(44) Muranevich, A. K. Heat Transfer in VO-MO (M= Ni, Co, Mn) Solid Solutions. *J. Am. Ceram. Soc.* **1978**, *61*, 257–259.

(45) Oliver, D. W. The Elastic Moduli of MnO. *J. Appl. Phys.* **1969**, *40*, 893–894.

(46) Towler, M.; Allan, N.; Harrison, N.; Saunders, V.; Mackrodt, W. C.; Aprà, E. Ab Initio Study of MnO and NiO. *Phys. Rev. B* **1994**, *50*, 5041–5054.

(47) Ling, C.; Banerjee, D.; Song, W.; Zhang, M.; Matsui, M. First-Principles Study of the Magnesiation of Olivines: Redox Reaction Mechanism, Electrochemical and Thermodynamic Properties. *J. Mater. Chem.* **2012**, *22*, 13517–13523.